Biomaterials Advances 133 (2022) 112609

Contents lists available at ScienceDirect

Biomaterials Advances

journal homepage: www.elsevier.com/locate/bioadv

Incorporation of magnesium oxide nanoparticles into electrospun membranes improves pro-angiogenic activity and promotes diabetic wound healing

Mingyue Liu [a,1], Ruilan Wang [b,1], Jiajie Liu [c,1], Weixing Zhang [b], Zhengni Liu [c], Xiangxin Lou [a], Huali Nie [a], Hongsheng Wang [a], Xiumei Mo [a], Ahmed I. Abd-Elhamid [a], Rui Zheng [d,*], Jinglei Wu [a,*]

[a] Key Laboratory of Science and Technology of Eco-Textile, Ministry of Education, College of Chemistry, Chemical Engineering and Biotechnology, Donghua University, Shanghai 201620, PR China
[b] Department of Critical Care Medicine, Shanghai General Hospital, Shanghai Jiao Tong University School of Medicine, Shanghai 201620, PR China
[c] Department of Hernia and Abdominal Wall Surgery, Shanghai East Hospital, Tongji University, Shanghai, 200120, PR China
[d] Department of Dermatology, Shanghai Ninth People's Hospital, Shanghai Jiao Tong University School of Medicine, 639 Zhi Zao Ju Road, Shanghai, 200011, PR China

ARTICLE INFO

Keywords:
Electrospun membrane
MgO nanoparticle
Diabetic wound
Bioactivity
Angiogenesis

ABSTRACT

Deficient angiogenesis is the major abnormality impairing the healing process of diabetic wounds. Electrospun nanofiber membranes have shown promise for wound dressing. A prerequisite for electrospun membranes to treating diabetic wounds is the capacity to promote angiogenesis of wounds. Current approaches are mainly focused on the use of pro-angiogenic growth factors to enhance the angiogenic properties of electrospun membranes. Despite improved angiogenesis, both the incorporation of growth factors into electrospun nanofibers and maintenance of its activity in the long term is of technical difficulty. We herein report an electrospun membrane made of polycaprolactone (PCL)/gelatin/magnesium oxide (MgO) nanoparticles (PCL/gelatin/MgO), which releases magnesium ions (Mg^{2+}) to enhance angiogenesis. MgO-incorporated membranes promote the proliferation of human umbilical vein endothelial cells and upregulate vascular endothelial growth factor (VEGF) production in vitro. Subcutaneous implantation study in a rat model demonstrates that the MgO-incorporated membrane shows a faster degradation profile and elicits moderate immune responses that gradually resolve. Upon subcutaneous implantation, PCL/gelatin/MgO membranes allow robust blood vessel formation as early as one week after surgery, and the newly formed capillary networks enrich within the degrading membrane over time. PCL/gelatin/MgO membranes significantly accelerated diabetic wound healing by suppressing inflammatory responses, promoting angiogenesis, and boosting granulation formation. Taken together, these results are implicative to rationally designing magnesium-incorporated electrospun membranes with improved pro-angiogenic activity for treating diabetic wounds.

1. Introduction

Chronic nonhealing wounds are the major complication of trauma for diabetic patients, which affects the life quality of patients and causes morbidity and mortality [1]. Diabetic wound microenvironment is hallmarked by abnormally elevated inflammation, imbalanced expression of growth factors and cytokines, insufficient neovascularization, and deficient accumulation of granulation tissue. Deficiency in angiogenesis is regarded as the primary abnormality for chronic diabetic wounds because it accounts for insufficient nutrient and oxygen supply that leads to scarce granulation formation [2]. Current approaches mainly target these abnormal alterations and revert them to normality to promote diabetic wound healing [1,3]. For instance, local sustained release of growth factors including VEGF [4], connective tissue growth factor (CTGF) [5], epithelial growth factor (EFG) [6], and basic fibroblast growth factor (bFGF) [7,8] have shown to accelerate diabetic wound closure. Administration of stem cells [9], microRNA [10], and exosomes [11] can also effectively ameliorate the hostile microenvironment of diabetic nonhealing wounds. Despite improved diabetic wound healing, the usage of exogenous growth factors/cytokines and cells is limited by storage, cost, uncertain dosage, and safety consideration. This necessitates effective therapeutics that provide bioactivity to improve neovascularization of diabetic wounds.

Magnesium is the fourth abundant element in the human body and the second most prevalent intracellular cation and plays critical roles in maintaining homeostasis and in regulating cellular events such as ion channels, enzyme activities, DNA stabilization, and proliferation and differentiation of cells [12,13]. Magnesium-based materials are attracting increasing interest for tissue engineering and regenerative medicine applications, e.g.

* Corresponding authors.
E-mail addresses: 115057@sh9hospital.org.cn (R. Zheng), jw@dhu.edu.cn (J. Wu).
[1] These authors contributed equally to this work.

http://dx.doi.org/10.1016/j.msec.2021.112609
Received 16 October 2021; Received in revised form 9 December 2021; Accepted 10 December 2021
Available online 14 December 2021

orthopedic implants, fillers, and stents [13–18]. For example, magnesium ceramics, e.g. magnesium oxide (MgO), magnesium phosphate (MgO-P_2O_5), and magnesium glasses (S_iO_2/MgO), show equivalent biological activity with magnesium alloys but without those side effects [13]. Composite scaffolds made from magnesium ceramics and polymeric materials, either in the forms of microsphere [19,20] or porous bone substitute [21–23], were found to boost the healing of critical-sized defects in preclinical studies. It is suggested that the promotive effects of magnesium ceramics on new bone formation might be associated with enhanced angiogenesis of regenerated bone tissues [21,24]. These reports indicate that magnesium ceramics could be of great pro-angiogenic properties.

Electrospinning has been used to prepare nanofibers for a wide range of biomedical and regenerative medicine applications [25–27]. Numerous strategies have been recently adopted to improve the angiogenesis of electrospun scaffolds in vivo. Engineered vascularized constructs integrating scaffolds with cells and/or growth factors represent a simple approach to overcome these obstacles [28]. Endothelial cells and smooth muscle cells are the primary cells contributing to angiogenesis and vasculogenesis. Pre-seeded cells on electrospun scaffolds often suffer from low survival after implantation due to the harsh microenvironment in vivo [29]. Vascular endothelial growth factor (VEGF) is the dominant growth factor that governs the process of angiogenesis by enhancing the proliferation and migration of endothelial cells and promoting tube formation. Controlled release of VEGF from electrospun core-shell nanofibers is an alternative to engineered vascularized constructs, while the major impediment to this approach is the relatively short half-life of VEGF [28,30–32].

The combination of magnesium-based materials with polymers to fabricate nanofiber membranes via electrospinning has gained increasing attention recently [33–37]. These composite nanofibers capitalize on the favorable properties of both magnesium ceramics and polymers, which enables them to superior biological activities for many biomedical and tissue engineering applications [33]. Electrospun scaffolds containing magnesium metallic particles [34] or MgO nanoparticles [33,38] promote cell attachment and proliferation and metabolic activity and mitigate inflammatory tissue responses to electrospun PCL alone scaffolds [35]. PCL/gelatin/MgO membranes pre-seeded with endometrial stem cells significantly promote healing processes of full-thickness skin wounds in a rat model [36]. Our recent studies demonstrates that poly(L-lactic acid) (PLA)/gelatin/MgO membranes facilitate periodontal regeneration [37] and PCL/gelatin/MgO membranes promote the healing process of infected wounds [38]. We therefore proposed that pro-angiogenic properties of MgO-incorporated membranes could benefit diabetic wound healing by improving angiogenesis. In this study, we prepared a PCL/gelatin/MgO nanofiber membrane by electrospinning and assessed its bioactivity through in vitro and in vivo studies, evaluated its capacity for promoting wound healing in a diabetic rat model.

2. Materials and methods

2.1. Materials

Glacial acetic acid, magnesium oxide nanoparticles (MgO, ~50 nm diameter), and 2,2,2-trifluoroethanol (TFE) were purchased from Shanghai Aladdin Bio-Chem Technology Co., LTD. PCL (M_n 80 kDa) and type A gelatin from porcine skin (~300 g Bloom) were provided by Sigma-Aldrich. Streptozotocin (STZ) and sodium citrate were provided by Shanghai Macklin Biochemical Co., Ltd. All chemicals were used as received without purification.

2.2. Preparation and characterization of electrospun membranes

PCL/gelatin/MgO nanofiber membrane was prepared by electrospinning as described in our previous study [37]. PCL and gelatin were dissolved in TFE/acetic acid (0.2%, *v*/v) [39] at the polymer concentration of 10% (wt/v) with PCL/gelatin ratio of 8:2. MgO nanoparticles were added to the as-prepared PCL/gelatin solution and sonicated for 30 min to allow a PCL/gelatin/MgO preparation with homogenous dispersion of MgO nanoparticles (0.5% wt/v). The preparation was fed at 1.5 mL/h and electrospun at a high voltage of 15 kV and collected by a slow-speed mandrel (60 rpm) at 10 cm to obtain PCL/gelatin/MgO membrane. An electrospun membrane made from PCL/gelatin solution without adding MgO nanoparticles was denoted as PCL/gelatin and served as a control.

Surface morphology and chemical compositions of electrospun membranes were analyzed by a scanning electron microscope (SEM, Hitachi, TM-1000, Japan) with an ESM spectrometer. Fiber diameters of electrospun membranes were measured from SEM images using ImageJ. The average pore size and pore size distribution of electrospun nanofiber membranes were measured by an automated Capillary Flow Porometer (CFP-1100AI, Porous Materials Inc., USA).

The pH variation and release of magnesium ions of electrospun membranes incubation were performed by incubating membranes in 0.9% saline at 37 °C according to our previous study [37]. The pH values of incubations were determined by a digital pH meter ($n = 4$). The incubated solution was collected for analysis and replaced by fresh saline at predesigned time points. The concentration of magnesium ion was determined by an inductively coupled plasma atomic emission spectroscopy (ICP-AES) (Prodigy Plus, Teledyne Leeman Labs, USA) ($n = 5$).

The moisture permeability and water absorption of electrospun membranes were assessed by measuring their water vapor transmission rates (WVTRs) as previously described [40]. Briefly, electrospun membranes were cut into discs to fit the mounts of cylindrical measuring cups. Disc membranes were mounted on the mouth of measuring cups containing deionized water and were maintained in a 37 °C incubator with 50% humidity for 24 h.

Electrospun membranes were tailored into strips (10 × 40 mm) and incubated in phosphate buffered saline (PBS) at 37 °C for 24 h for uniaxial tensile testing. Strip specimens were mounted in the grips of a universal materials testing machine (Instron 5567, Norwood, MA) with a 200 N load cell and were tested at a crosshead speed of 10 mm/min until failure. Ultimate tensile strength (UTS) was determined by the maximum tensile strength before failure and Young's modulus was calculated as the slope of the initial 5% linear portion from the stress-strain curve ($n = 5$).

2.3. In vitro assessments

2.3.1. Cell seeding

NIH 3T3 fibroblasts and human umbilical vein endothelial cells (HUVEC) were kindly provided by the Cell Bank of Chinese Academy of Science. Both cells were maintained and expanded in high glucose DMEM supplemented with 10% fetal bovine serum and 1% penicillin/streptomycin antibiotics. Electrospun membranes were punched to discs with various diameters to different sized well plates. Disc samples were immersed in 70% ethanol for 1 h and then irradiated under UV (12 h for each side) for disinfection. NIH 3T3 fibroblasts and HUVECs were separately seeded onto the surface of electrospun membranes at the density of 2×10^4 cells/cm^2 in 24-well plates. Cell culture was maintained in a 37 °C incubator with 95% humidity and 5% CO_2. Medium was refreshed every other day.

2.3.2. Cytocompatibility of electrospun membranes

Cell viability and proliferation on electrospun membranes in 24 well plates were assessed by live/dead staining and CCK-8 assay, respectively. At days 1, 4, and 7, cell-seeded membranes were stained with calcein-AM and propidium iodide for 30 min at 37 °C and visualized by a fluorescence microscope (DMi 8, Leica, Germany) ($n = 3$). For proliferative assessment, cell-seeded membranes were incubated with CCK-8 assay at 37 °C for 1.5 h, and then 100 μL supernatant of each well was read at 450 nm using a plate reader (Multiskan MK3, Thermo, USA) ($n = 5$).

The morphology of NIH 3T3 fibroblasts and HUVECs on electrospun membranes was observed by scanning electron microscopy. Samples were rinsed with PBS, fixed with 4% paraformaldehyde, dehydrated with gradient ethanol, and dried at room temperature. After sputter-coating with gold, samples were observed under a scanning electron microscope (Phenom, Netherlands).

2.3.3. Measurement of vascular endothelial growth factor

HUVECs were seeded on electrospun membranes at a density of 7.5×10^4 cells/cm^2 in 12-well plates. Cell culture supernatants were collected at predetermined time points and stored at −80 °C until assay. Accumulated VEGF was measured by ELISA according to the manufacturer's instructions ($n = 4$).

2.4. Diabetic wound healing model and treatments

2.4.1. Diabetic rat model induced by STZ

Male Sprague Dawley (SD) rats (~180 g) were obtained from Shanghai JSJ Lab Animal Center and were housed in a laboratory with a temperature of 22–25 °C and 40–70% humidity at a light-dark cycle of 12 h. After 10 h of fasting subjects, diabetic Mellitus rat models were prepared by the administration of a single dose of STZ (65 mg/kg, i.p.) according to a well-established protocol [41]. After 10 days, blood glucose was measured and animals with blood glucose greater than 14 mmol/L were considered successful diabetic rats and included for subsequent studies.

2.4.2. Surgical procedures

Animal experiments and procedures were reviewed and approved by the ethical committee of Donghua University (No. DHUES-STCSM-2020-01) and were performed in accordance with the Guide for the Care and Use of Laboratory Animals (National Institutes of Health, 8th Edition, revised 2011). Diabetic rats were anesthetized by intramuscular injection of Zoletil (40 mg/kg) and 2% Xilazina (3 mg/kg) and fixed on a sterile drape for surgery. The dorsal area was shaved and disinfected with 70% isopropyl alcohol. Paired symmetrical round full-thickness wounds (10 mm in diameter, six wounds for each animal) were created on the dorsum using a scalpel. Wounds were received various dressing treatments (PCL/gelatin membranes or PCL/gelatin/MgO membranes) and then covered with a sterile adhesive dressing (3 M Tegaderm™, MN). Considering that magnesium ions might enter the blood circulation and thus improve wound healing, each animal was exclusively treated with the same membranes. Wounds that did not receive electrospun membrane treatment but were directly covered by sterile adhesive dressing were set as a control group. Forty-five diabetic rats with blood glucose greater than 14 mmol/L were randomly divided into three groups (fifteen rats for each group). Three animals were used for each group at each time point.

2.4.3. Wound closure and gene expression

For each group, two wounds of each animal were recorded with a digital camera at each timepoint. The sizes of wounds were measured from recorded images using ImageJ and normalized to that of the original sizes (day 0) to calculate wound closure rates over time ($n = 6$ for each group).

At day 7 after surgery, for each group, one wound was excised from each animal and frozen in liquid nitrogen. Total RNA was extracted from wounds using Trizol according to the manufacturer's instructions (Sangon Biotech Co., Ltd., Shanghai, China). cDNA was synthesized by reversely transcribed from total RNA using RevertAid First Strand cDNA Synthesis kit (Thermo Fisher Scientific). Quantitative real-time PCR was carried out using NovoStart® SYBR qPCR SuperMix Plus (Novoprotein Scientific Inc., Shanghai, China) in an Applied Biosystems™ 7500 real-time PCR system and analyzed by comparative Ct quantification method (ΔΔCt). The target and sequences of primers are shown in Table 1. The expression levels of IL-1β, TNF-α, TGF-β1, and α-SMA genes were relative to glyceraldehyde 3-phosphate dehydrogenase (GAPDH) and normalized to the levels of the control group ($n = 3$ for each group).

2.4.4. Histological and immunofluorescent analyses

At days 3, 7, and 14 after surgery, wounds were fixed in 4% formaldehyde, embedded with paraffin, and then sliced into 5 μm sections. Hematoxylin & eosin (H&E) and Masson's Trichrome staining were performed following standard protocols and scanned using a digital slide scanner (PRECICE 500×).

Table 1
Primer sequences of genes for qRT-PCR analysis.

Gene	Primer sequence(5′-3′)	Accession number
TGF-β1	F:5' GGACCGCAACAACGCAATCTA 3' R:5' AGACAGCCACTCAGGCGTATC 3'	NM_021578.2
α-SMA	F:5' AACTGGTATTGTGCTGGACTCTG 3' R:5' CTCAGCAGTAGTCACGAAGGAATA 3'	NM_031004.2
IL-1β	F:5' CTGTGACTCGTGGGATGATGAC 3' R:5' CCACTTGTTGGCTTATGTTCTGTC 3'	NM_031512.2
TNF-α	F:5' GCCACCACGCTCTTCTGTCTA 3' R:5' CGCTTGGTGGTTTGCTACGA 3'	NM_012675.3
GAPDH	F:5' CCACCACGCTCTTCTGTCTACTG 3' R:5' TGGGCTACGGGCTTGTCACT 3'	NM_017008.4

For immunofluorescence, paraffin-embedded sections were deparaffinized by xylene, dehydrated with gradient ethanol, and rehydrated for antigen retrieval. After quenching with 3% hydrogen peroxide and blocked with 5% bovine serum albumin, sections were incubated with primary antibodies of anti-CD31 (1:200; Abcam,), anti-CD68 (1:500; Abcam), anti-CD86 (1:300, Proteintech), and anti-CD206 (1:1000, Proteintech) at 4 °C overnight. After incubation with biotinylated secondary antibodies, sections were visualized using Nikon DS-U3 system.

2.5. Evaluation of biocompatibility

2.5.1. Subcutaneous implantation

Electrospun membranes were tailored to 14 mm discs and subcutaneously implanted in male SD rats to evaluate their biocompatibility. Membranes were disinfected by immersing in 70% ethanol for 30 min, followed by UV irradiation (30 min each side). Animals were anesthetized by intramuscular injection of Zoletil (40 mg/kg) and 2% Xilazina (3 mg/kg). The dorsal area of rats was shaved and disinfected with 70% ethanol. For subcutaneous implantation, a pocket was created by the incision of the midline, inserted with a disc membrane, and sutured by 5–0 sutures. Each animal received a PCL/gelatin membrane and a PCL/gelatin/MgO membrane. Three animals were euthanized at each time point and a total of twelve animals were used for the biocompatibility study. Membranes were retrieved for analysis at predetermined endpoints of 3, 7, 14, and 28 days after surgery. Implanted membranes along with adjacent tissues were retrieved, fixed by 4% paraformaldehyde, paraffin-embedded, and sectioned into 5 μm slides for staining.

2.5.2. Histological analyses

The paraformaldehyde-fixed and paraffin-embedded sections of retrieved electrospun membranes were H&E and Masson's trichrome stained for histological analysis. Depths of cell infiltration into electrospun membranes were measured from H&E staining images and thicknesses of fibrous capsule surrounding implanted electrospun membranes were measured from Masson's Trichrome staining images using Image J ($n = 3$ for each group). For the determination of infiltration depth and fibrous capsule thickness, at least 8 random views of histological images for each membrane at each time point were measured and averaged.

2.5.3. Immunohistochemical analysis

For immunohistochemical analysis, the paraffin of paraffin-embedded slides was removed using EZDeWax solution (Biogenex Lab, San Ramon, CA) and pretreated as follow: rehydrated with gradient ethanol, briefly rinsed with deionized water, immersed in 0.3% H_2O_2, blocked with 3% bovine albumin serum, and then washed with phosphate-buffered saline. Pretreated slides were then stained with mouse anti-rat monoclonal antibodies of anti-CD68 (1:200; Santa Cruz Biotechnology), anti-CD11b (1:100, Santa Cruz Biotechnology), and anti-CD31 (1:200; Abcam) to identify the presence of pan-macrophages, leukocytes, and vascular endothelial cells, respectively. Slides were then incubated with a 1:100 dilution of peroxidase-conjugated goat anti-mouse secondary antibody (Jackson ImmunoResearch Laboratories, PA) and developed with DAB (Sigma) according to the manufacturer's instructions.

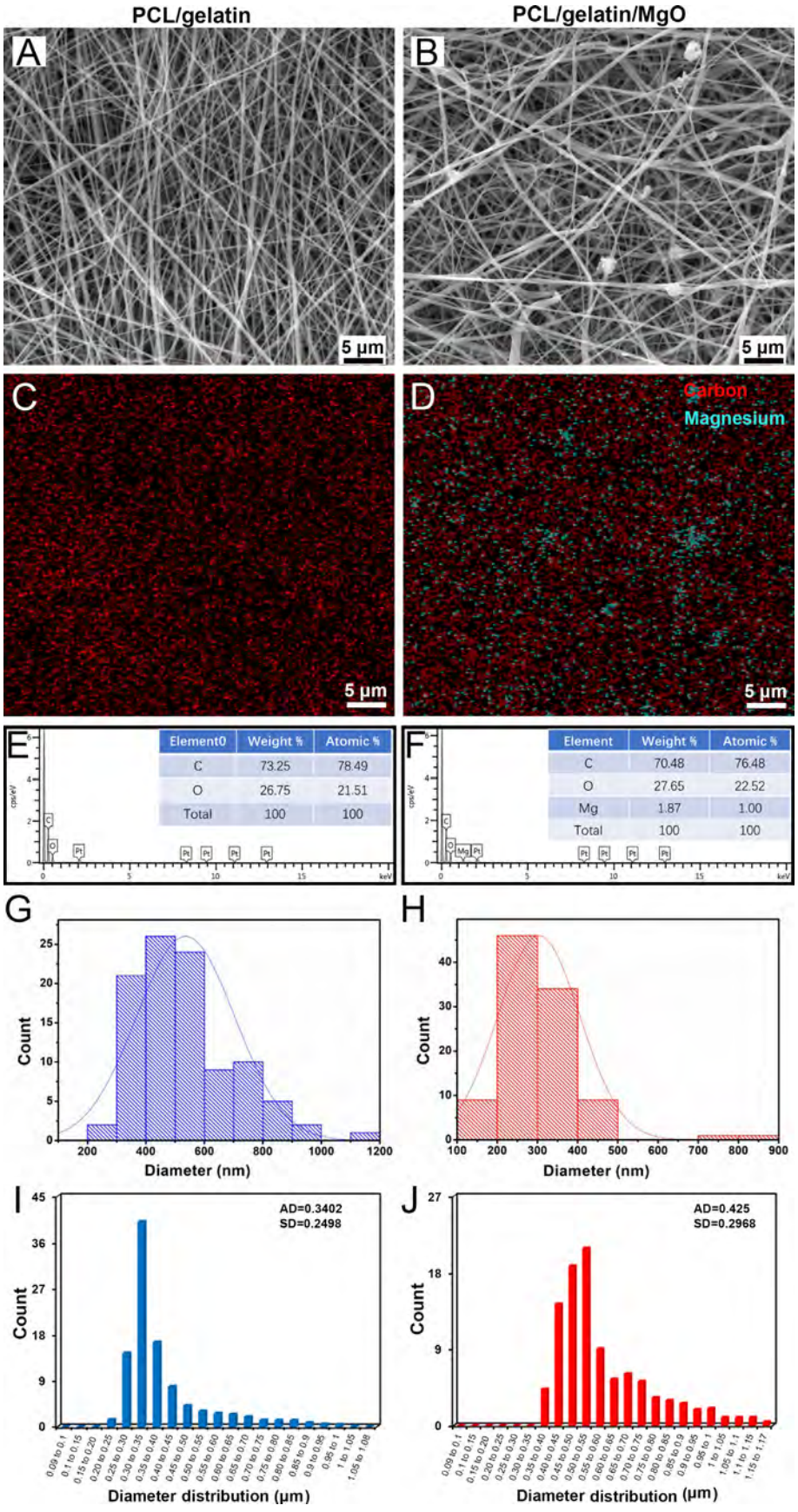
PCL/gelatin
PCL/gelatin/MgO
A
B
5 μm
5 μm
C
D
Carbon
Magnesium
5 μm
5 μm
E
Element0 Weight % Atomic %
C 73.25 78.49
O 26.75 21.51
Total 100 100
F
Element Weight % Atomic %
C 70.48 76.48
O 27.65 22.52
Mg 1.87 1.00
Total 100 100
G
Count
Diameter (nm)
H
Count
Diameter (nm)
I
AD=0.3402
SD=0.2498
Count
Diameter distribution (μm)
J
AD=0.425
SD=0.2968
Count
Diameter distribution (μm)

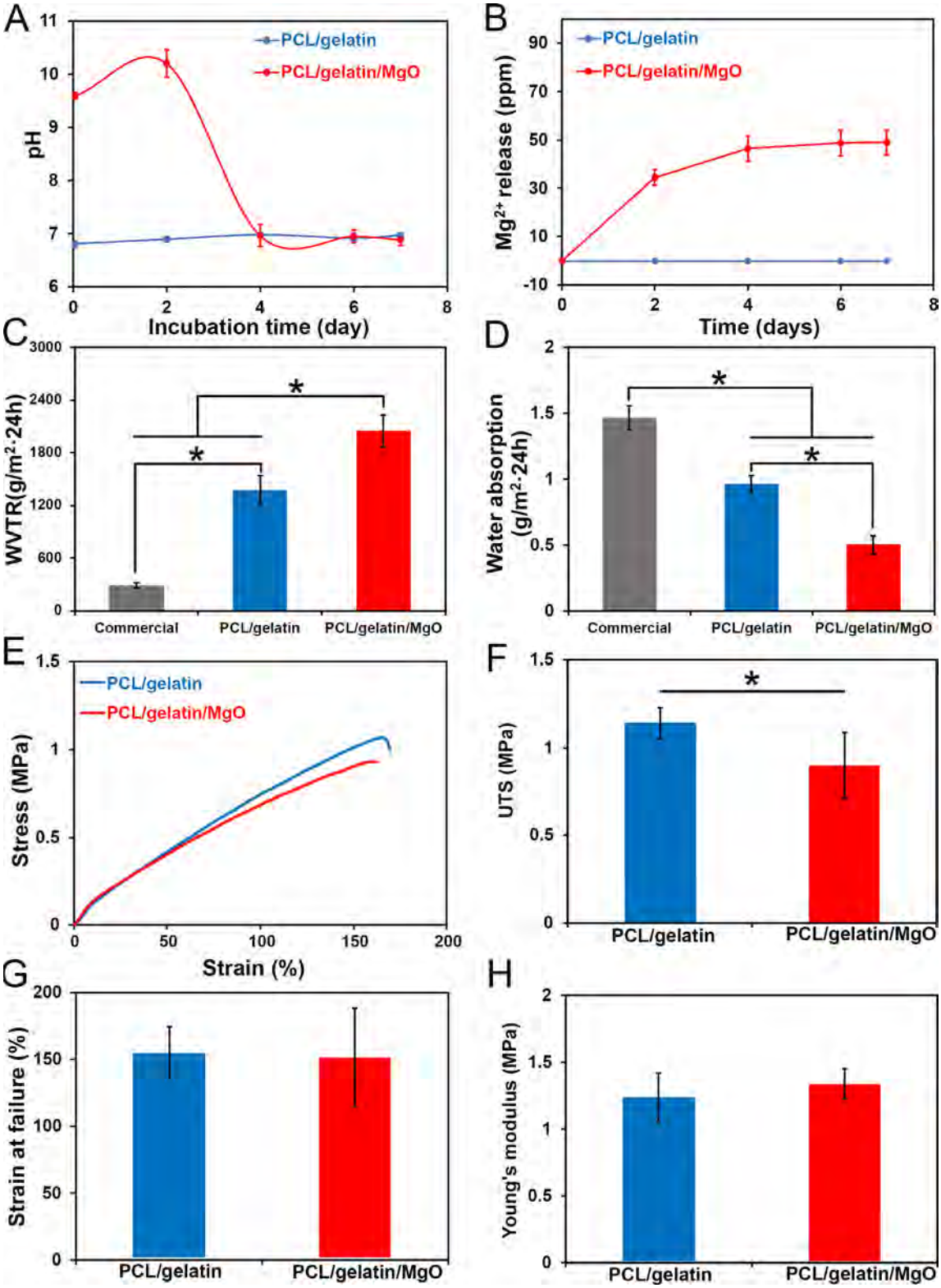

Fig. 2. pH variation (A), Mg^{2+} release (B), WVTR (C), water absorption (D), and tensile strength properties (E, F, G, and H) of electrospun membranes. The PCL/gelatin/MgO membrane shows a higher stress-strain curve (E) with greater UTS (F) and comparable breaking strain (G) and Young's modulus (H) compared with the PCL/gelatin membrane. One-way ANOVA with Tukey's post hoc test for Cand D; unpaired Student's *t*-test for F, G, and h; * indicates $p < 0.05$.

Fig. 1. Ultrastructure, element analysis, fiber diameter, and pore size of electrospun membranes. SEM images reveal a similar dense fibrous configuration of PCL/gelatin (A) and PCL/gelatin/MgO (B) membranes, while the bead-like aggregation of MgO nanoparticles can be observed in the latter membrane. Element mapping (C, D, E and F) shows homogeneous distribution of carbon and magnesium. Occasional local magnesium aggregation is found within the PCL/gelatin/MgO membrane (D). Fiber diameter (G and H) and pore size (I and J) distribution of electrospun PCL/gelatin (G and I) and PCL/gelatin/MgO (H and J) membranes.

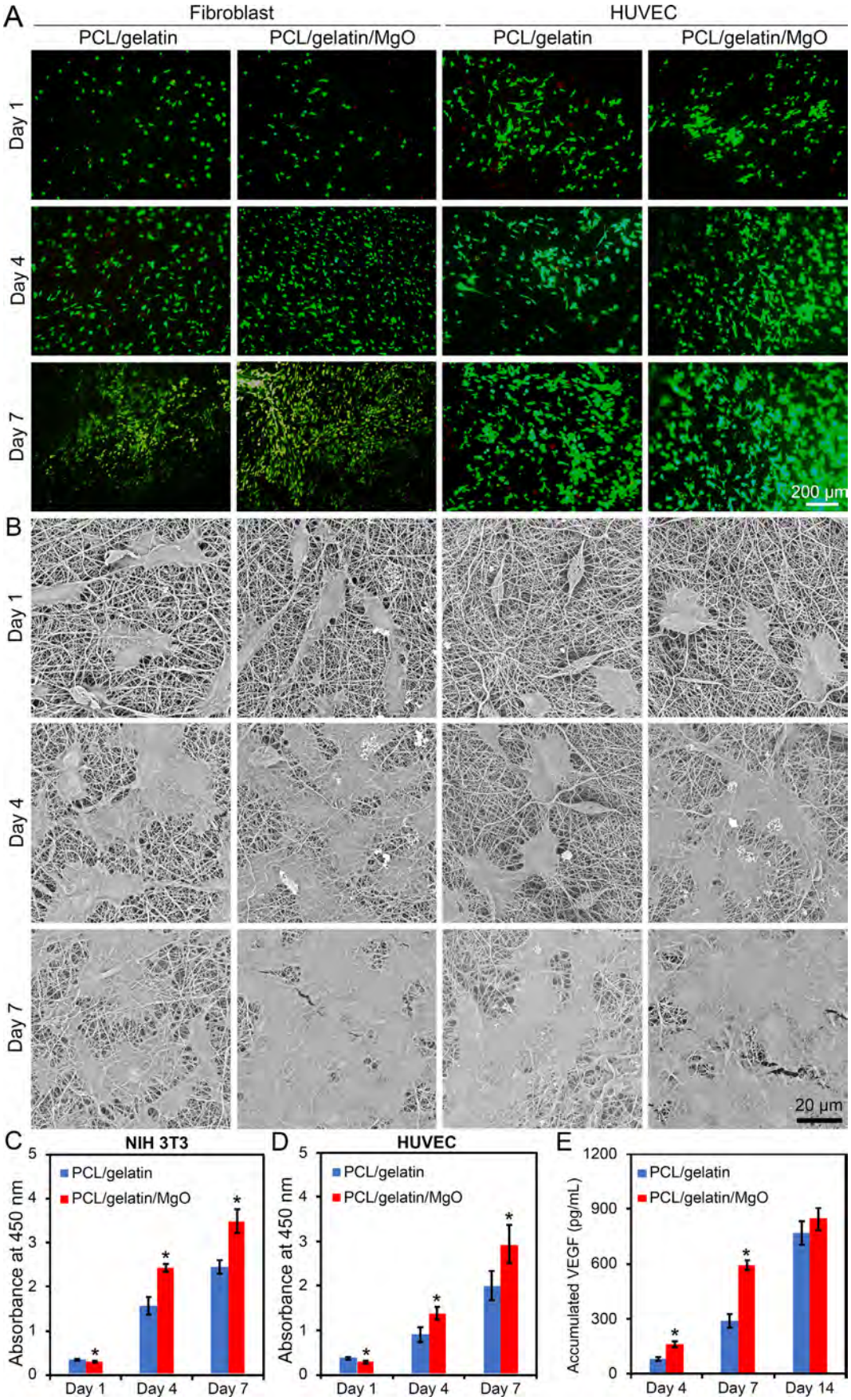
A
Fibroblast
HUVEC
PCL/gelatin
PCL/gelatin/MgO
PCL/gelatin
PCL/gelatin/MgO
Day 1
Day 4
Day 7
200 μm
B
Day 1
Day 4
Day 7
20 μm
C
NIH 3T3
PCL/gelatin
PCL/gelatin/MgO
Absorbance at 450 nm
Day 1
Day 4
Day 7
D
HUVEC
PCL/gelatin
PCL/gelatin/MgO
Absorbance at 450 nm
Day 1
Day 4
Day 7
E
PCL/gelatin
PCL/gelatin/MgO
Accumulated VEGF (pg/mL)
Day 4
Day 7
Day 14

2.6. Statistical analysis

Data were present as means ± standard deviations and were analyzed by unpaired Student's *t*-test or one-way or two-way analysis of variance (ANOVA) where appropriate. Statistical significance was considered at $p < 0.05$.

3. Results

3.1. Properties of electrospun membranes

PCL and gelatin were dissolved in TFE solution, which was either directly electrospun or added with MgO nanoparticles for electrospinning to prepare nanofiber membranes. The addition of MgO nanoparticles into PCL/gelatin solution resulted in a milky suspension that was stable for several days (Fig. S1), which allows smooth electrospinning and homogeneous nanoparticle distribution in nanofibers. SEM images revealed that both PCL/gelatin (Fig. 1A) and PCL/gelatin/MgO (Fig. 1B) membranes showed randomly oriented dense nanofibers with small interfiber distance. PCL/gelatin nanofibers appeared to be rigid, while PCL/gelatin/MgO nanofibers were less straight and showed locally coiled texture. Individual MgO nanoparticles were either fully embedded within nanofibers or aggregated to microparticles attaching to nanofibers (Fig. 1B). EDS mapping images (Fig. 1C and D) showed that carbon and magnesium elements were homogeneously distributed within electrospun membranes, while occasional aggregation of magnesium elements could be observed within the PCL/gelatin/MgO membrane (Fig. 1D). The PCL/gelatin membrane had a relatively uniform fiber diameter (Fig. 1E) and smaller pore size (Fig. 1G) than that of the PCL/gelatin/MgO membrane (Fig. 1F and H).

The incorporation of MgO nanoparticles into electrospun membranes resulted in an alkaline incubation (~ pH = 10) within 2 days, which were then declined to a neutralized pH of 7 comparable to the PCL/gelatin membrane (Fig. 2A). The pH variation was accompanied by Mg^{2+} release for the PCL/gelatin/MgO membrane. Interestingly, the PCL/gelatin/MgO membrane had a significantly greater WVTR (Fig. 2C) and smaller water absorption ability (Fig. 2D) compared with the PCL/gelatin membrane. This is likely due to its larger pore size that allows faster evaporation and holds less moisture. In addition, the PCL/gelatin/MgO membrane had a lower stress-strain curve (Fig. 2E) with a significantly smaller UTS (Fig. 2F) compared with the PCL/gelatin membrane. No significant difference in breaking strain (Fig. 2G) or Young's modulus (Fig. 2H) was observed between electrospun membranes.

3.2. Cytocompatibility of electrospun membranes

Cytocompatibility of electrospun membranes was assessed by live/dead staining, SEM, and CCK-8 assay (Fig. 3). Both NIH 3T3 fibroblasts and HUVECs were predominately alive (green) with a few dead cells (red) on electrospun membranes during culture (Fig. 3A). Fibroblasts were firmly attached to the electrospun nanofibers and showed increased coverage on electrospun membranes over time (Fig. 3B). HUVECs showed a predominant spindle shape on the PCL/gelatin membrane at day 1. In contrast, they exhibited polygonal shape and spread well on the PCL/gelatin/MgO membrane. Overall, both fibroblasts and HUVECs showed greater coverage on the PCL/gelatin/MgO membranes compared that on the PCL/gelatin membrane at days 4 and 7 (Fig. 3B). Fibroblasts (Fig. 3C) and HUVECs (Fig. 3D) similarly showed steady proliferation from day 1 to day 7. At day 1, the PCL/gelatin membrane supported significantly higher proliferation rates than the PCL/gelatin/MgO membrane. On the contrary, cells showed much higher proliferation rates on the PCL/gelatin/MgO membrane at subsequent endpoints (Fig. 3C and D).

3.3. VEGF accumulation

Endothelial cells are known to secrete vascular endothelial growth factors, which are quantified via ELISA assay and shown in Fig. 3E. The PCL/gelatin/MgO membrane stimulated HUVECs to produce a significantly greater amount of VEGF compared with the PCL/gelatin membrane at day 4 ($p = 0.0002$). The difference became even larger at day 7: the PCL/gelatin/MgO membrane accumulated one-fold more VEGF than the PCL/gelatin membrane. No significant difference in VEGF accumulation between the two membranes was found at day 14 ($p = 0.12$).

3.4. Diabetic wound healing

Excisional full-thickness skin wounds (10-mm diameter) of STZ-induced diabetic rats were made to evaluate the effects of electrospun membranes on diabetic wound healing. Wounds were examined 3, 7, 10, and 14 days after surgery (Fig. 4A). Wounds of the control group were swollen with bacterial infection, a common complication of chronic diabetic wounds, at day 3 and were slightly reduced to >80% and > 60% (Fig. 4B) of their original sizes at days 7 and 14, respectively. The PCL/gelatin membrane-treated wounds showed similar extents of healing as the control group. In contrast, wounds of the PCL/gelatin/MgO group showed clean wound beds (Fig. 4A) and experienced a significantly accelerated wound closure rate ($p < 0.05$) (Fig. 4B), leading to wound areas less than 40% of the original sizes.

The expression levels of pro-inflammatory genes, IL-1β and TNF-α, and pro-healing genes, TGF-β1 and α-SMA, were determined by qRT-PCR 7 days after injury (Fig. 4C). Wounds of the PCL/gelatin group showed comparable expression levels of pro-inflammatory and pro-healing genes to that of the control group ($p > 0.05$). The PCL/gelatin/MgO membrane significantly downregulated the expression levels of IL-1β and TNF-α ($p < 0.05$) and upregulated the expression levels of TGF-β1 and α-SMA ($p < 0.05$) compared with the control and PCL/gelatin groups. These results demonstrate the crucial role of incorporated MgO in mitigating inflammation and promoting healing processes.

H&E staining shows that none of these wounds had granulation formation at day 3 and the PCL/gelatin/MgO membrane-treated wound showed greater granulation thickness thereafter than the PCL/gelatin and control groups (Fig. 5A). Masson's Trichrome staining confirms that the granulation tissue of the PCL/gelatin/MgO group showed a relatively intensive blue colour at day 7 with respect to the other groups (Fig. 5B). Specifically, the bottom of granulation tissue was in dark blue than the upper layer, indicating that the collagen deposition during wound healing is an upward process from the muscular layer to the epithelium. At day 14, the PCL/gelatin/MgO membrane-treated wound showed organized, dense collagen networks in the granulation tissue.

Fig. 6 shows immunofluorescent staining of healing wounds at days 7 and 14. Wounds of the control group showed extensive macrophage (CD68 +) distribution within the granulation tissue, the PCL/gelatin membrane-treated wounds intermediated and the PCL/gelatin/MgO membrane-treated wounds had the least population of macrophages (Fig. 6A). On the contrary, the PCL/gelatin/MgO membrane-treated wounds had much more CD31 + cells compared with the other groups (Fig. 6A), demonstrating sufficient neovascularization within the granulation tissue. We further identified the phenotypes of macrophages by immunofluorescent staining of pro-inflammatory subpopulations (M1, CD86 +) and pro-healing subpopulations (M2, CD206 +) (Fig. 6B). M1 macrophages dominated in wounds of the control and PCL/gelatin groups, whereas M2 macrophages were the prevailing population in the PCL/gelatin/MgO group.

Fig. 3. Assessments of cytocompatibility. Live/dead staining (A) reveals that NIH 3T3 fibroblasts and HUVECs show good viability on electrospun membranes. Both cells show increased coverage on the surface of electrospun membranes over time (B). The PCL/gelatin/MgO membrane supported lower proliferation rates of fibroblasts (C) and HUVECs (D) at day 1 but much greater proliferation rates at days 4 and 7. n = 5, unpaired Student's *t*-test, * indicates $p < 0.05$ vs. PCL/gelatin. The PCL/gelatin/MgO membrane stimulates HUVECs to produce significantly greater VEGF at days 4 and 7 compared with the PCL/gelatin membrane. n = 4, unpaired Student's t-test, * indicates $p < 0.05$ vs. PCL/gelatin.

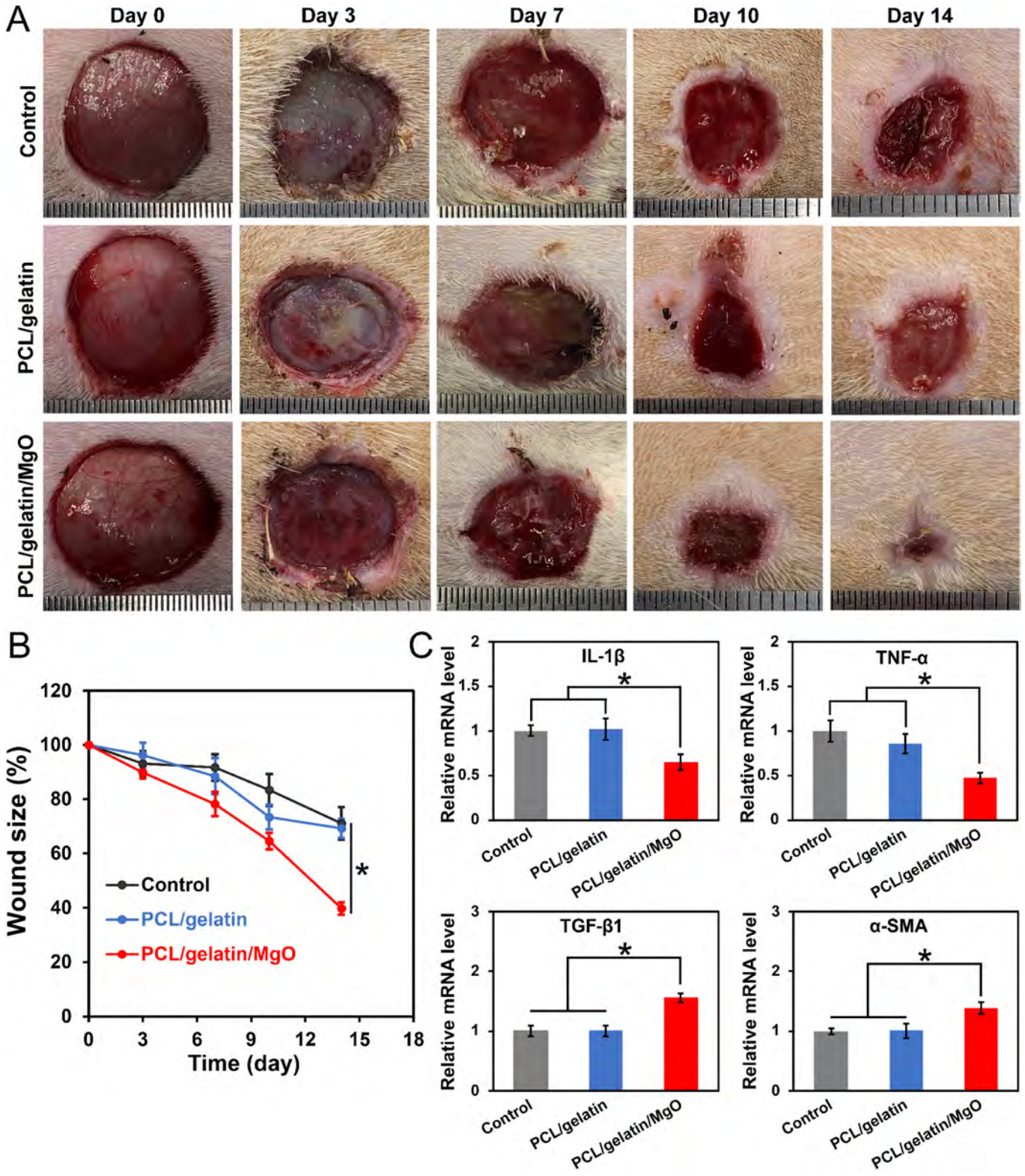

Fig. 4. Assessments of full-thickness defect wound healing in an STZ diabetic rat model. Gross appearance of diabetic wounds with electrospun membrane treatments for 14 days (A). The PCL/gelatin/MgO membrane effectively suppresses bacterial infection and reduces wound swelling. Wound closure curves (B) demonstrate that the PCL/gelatin MgO membrane significantly accelerates the healing process of diabetic wounds compared with the PCL/gelatin membrane and control groups. One-way ANOVA with Tukey's post hoc test, $n = 6$, * indicates $p < 0.05$. qRT-PCR analysis indicates that the PCL/gelatin/MgO membrane significantly downregulates the gene expression levels of IL-1β and TNF-α (C). Simultaneously, it significantly upregulates the pro-healing gene expression levels of TGF-β1 and α-SMA. One-way ANOVA with Tukey's post hoc test, $n = 3$, * indicates $p < 0.05$.

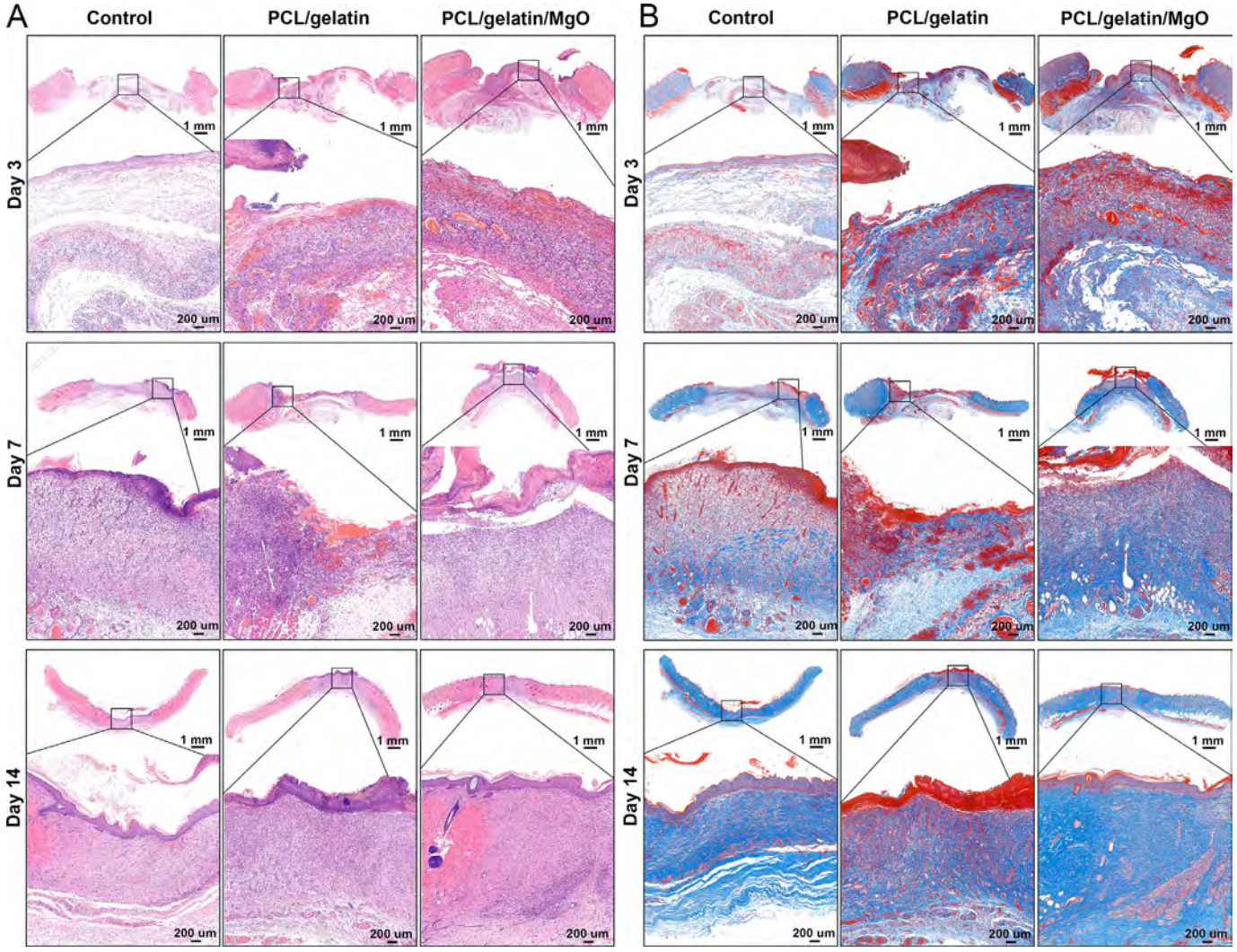

Fig. 5. Histological analysis of H&E (A) and Masson's Trichrome (B) staining of diabetic wounds receiving various treatments at days 3, 7, and 14 after surgery. The PCL/gelatin/MgO membrane induces earlier granulation tissue formation at day 3 and increased volume of granulation tissue almost filling up the defect at day 7 (A). Masson's Trichrome staining indicates that the PCL/gelatin/MgO membrane-treated wound shows relatively mature collagen deposition at day 14 in comparison to the control and PCL/gelatin groups (B).

3.5. Foreign body response to electrospun membranes

Electrospun membranes were subcutaneously implanted in a rat model and foreign body response (FBR) to membranes was assessed by histological and immunohistochemical analyses. H&E staining of explanted membranes showed that they were encapsulated by inflammatory cells and fibrous capsules (Fig. 7A). Inflammatory cells were mainly localized in the fibrous capsule at day 3 and gathered at the membrane-tissue interface of the PCL/gelatin membrane at day 7 and some of them fused to form foreign body giant cells (FBGCs) at day 14. A similar pattern of inflammatory cells surrounding the PCL/gelatin/MgO membrane was found at days 3 and 7, while they infiltrated a certain depth into the membrane at day 14. Cell infiltration into membranes was quantified by summing the infiltrated depths from both the muscle and skin sides. The PCL/gelatin/MgO membrane supported significantly higher cell infiltration compared with the PCL/gelatin membrane at days 7 ($p < 0.01$) and 14 ($p < 0.0001$) (Fig. 7C).

Fibrous capsule encapsulation of implanted electrospun membranes by host tissue was observed at day 3 and extended to 14 days as revealed by Masson's Trichrome staining (Fig. 7B). The fibrous capsule was mainly composed of dense collagen and inflammatory cells. The PCL/gelatin membrane had fibrous capsule thickness of 100 μm and did not change for up to 14 days. The fibrous capsule thickness of PCL/gelatin/MgO membrane was significantly reduced from 124 ± 17 μm at day 3 to 78 ± 14 μm at day 14 ($p < 0.0001$), indicating a gradually resolving inflammatory response over time. The PCL/gelatin/MgO membrane resulted in a slightly thicker fibrous capsule at day 3 but a thinner fibrous capsule at day 14 in comparison to the PCL/gelatin membrane (Fig. 7D).

Macrophage phenotype was determined by immunohistochemical staining (Fig. 8A and B) against CD68+ and CD11b + for identifying pan-macrophages and leukocytes, respectively. Both membranes showed pan-macrophages presence at day 7 while the localization and density of pan-macrophages differed. Specifically, pan-macrophages were predominantly localized at the exterior of fibrous capsule apical to the PCL/gelatin membrane at day 7 (Fig. 8A). In contrast, pan-macrophages showed a higher density within the fibrous capsule and gathered at the membrane-capsule interface at day 7 for the PCL/gelatin/MgO implant, indicating an elevated inflammatory response compared with the PCL/gelatin implant. The inflammatory response to implants was reduced at day 14 but greatly elevated at day 28 for both electrospun membranes, as shown by first decline with a subsequent increase in the number of pan-macrophages from day 14 to day 28. A significant reduction in the thickness of the PCL/gelatin/MgO membrane was observed while the PCL/gelatin membrane did not show reduced thickness at the same course.

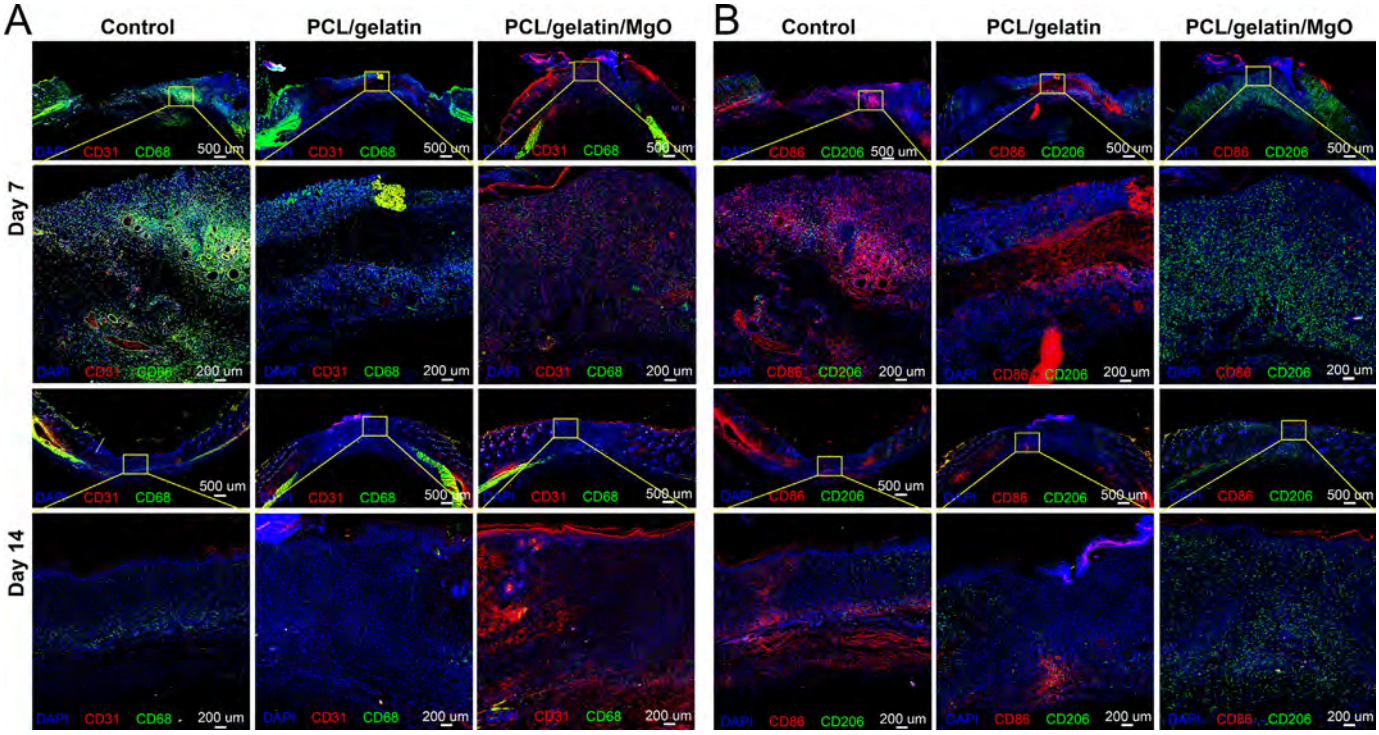

Fig. 6. Immunofluorescent staining of diabetic wounds to show CD68 + pan-macrophages (green stain in A), CD31 + cells (red stain in A), and CD86 + macrophages M1 (red stain in B), CD206 + M2 (green stain in B) at days 7 and 14 after surgery. The PCL/gelatin/MgO membrane-treated wound shows the strongest angiogenesis as indicated by CD31 + cells and the least inflammatory responses as evidenced by CD68 + pan-macrophages (A). It also promotes early M1/M2 switch as shown by the general presence of CD206 + macrophages at day 7 (B).

The majority of infiltrating cells into electrospun membranes were CD11b positive (CD11b +) cells, a population of many leukocytes including monocytes, neutrophils, natural killer cells, granulocytes, and proinflammatory macrophages [42,43]. CD11b + cells showed little infiltration (less than 100 μm) into the PCL/gelatin membrane and accumulated to form a dense band surrounding the implant for up to 28 days (Fig. 8B). In contrast, CD11b + cells gradually infiltrated into the PCL/gelatin/MgO membrane. CD11b + cells infiltrated approximately 100 μm from both sides at day 7 and then halted until 14 days. Subsequently, intense infiltration of CD11b + cells into the PCL/gelatin/MgO membrane was observed, allowing a fully infiltrated membrane at day 28.

3.6. Angiogenesis of implanted membranes

Angiogenesis of subcutaneously implanted membranes was assessed by immunohistochemical staining of CD31 positive endothelial cells of blood vessels (Fig. 8C). There was no capillary formation after 14 days and capillaries were scarce within the implanted PCL/gelatin membrane after 28 days. Newly formed capillaries were observed within the implanted PCL/gelatin/MgO membrane and its surrounding capsule tissues as early as day 7. Increased numbers of capillaries within the PCL/gelatin/MgO membrane were found thereafter until 28 days, indicating enhanced angiogenesis of matured vascular network formation.

4. Discussion

The incorporation of MgO nanoparticles into electrospun membranes alters their physicochemical properties. We and other groups have demonstrated that incorporated MgO nanoparticles within electrospun nanofibers improve tensile strengths of electrospun membranes [33,36,37]. The reinforcement effect can be attributed to the effective transfer of stress between polymer chains and MgO nanoparticles [37]. However, these results were obtained by determining MgO-incorporated membranes in the dry state, which does not represent their applicability in clinical practice. In this study, we determined the tensile properties of electrospun membranes in the wet state that is more relevant to clinical application. Our result shows that the PCL/gelatin/MgO membrane has a UTS approximating that of human skin. Together with its ~200% breaking strain, the PCL/gelatin/MgO membrane exhibits good flexibility and serves great as wound dressings [38]. Another change associated with MgO hydrolysis is the elevation in pH of the local environment surrounding the PCL/gelatin/MgO membrane. This is because MgO hydrolyzes to generate magnesium hydroxide that causes an alkaline microenvironment (Fig. 2A), which downregulates the proliferation of fibroblasts (Fig. 3C) and endothelial cells (Fig. 3D) at the early time point of in vitro culture. MgO hydrolysis-induced local alkaline microenvironment also results in the upregulated early inflammation upon implantation (Figs. 7 and 8). The incubation of PCL/gelatin/MgO membrane shows a neutralized pH after a few days, which is due to exhausted MgO as evidenced by the peaked release of Mg^{2+} at day 4 (Fig. 2B). Our previous report shows that self-neutralization of MgO-incorporated membranes could be achieved by using PLA, a polymer that generates acidic products during degradation, which neutralizes MgO hydrolyzed alkaline products [37]. While the self-neutralization approach is efficient to circumvent early altered pH microenvironment, it could have long-term detrimental effects. MgO hydrolyzes quickly and mainly occurs during the first few days, but PLA degradation persists and continues to produce acidic products [44–46]. Accumulation of acidic products in the local microenvironment will lead to chronic inflammation [47]. Therefore, for consideration of long-term safety, we selected PCL to prepare electrospun MgO-incorporated membranes.

Rapid vascularization and angiogenesis of regenerating tissues remain the primary limiting step of tissue-engineered implants for regenerative medicine applications [48,49]. The diffusion limit for nutrients and oxygen from blood vessels to their surrounding tissues is estimated to be 200 μm, accordingly, cells predominantly reside such a distance within a capillary bed [43,50]. It is critical for implants to quickly form vascular networks upon implantation, which facilitates efficient transfer of oxygen, and nutrients from the extracellular milieu to resident cells and remove metabolic

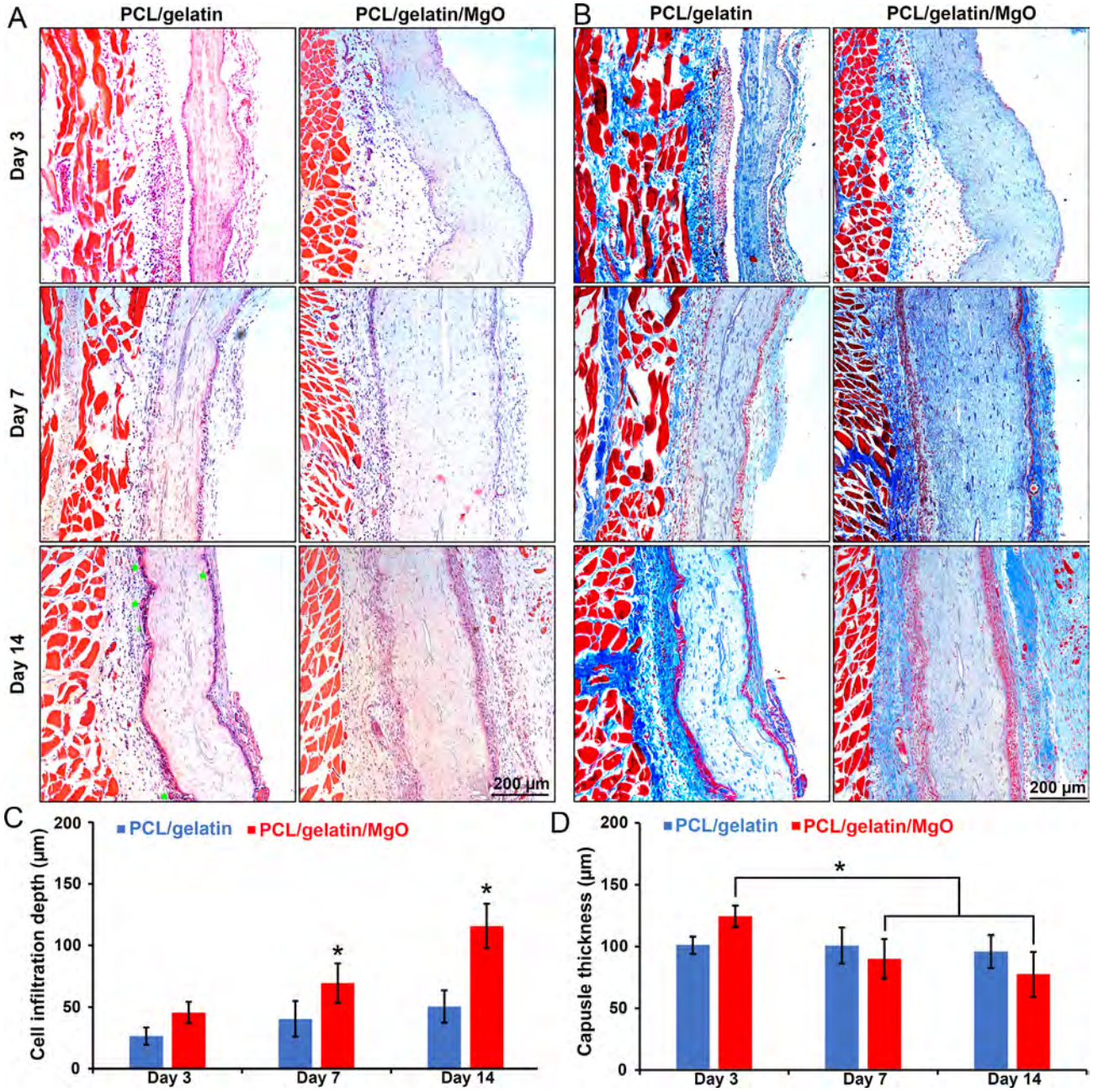

Fig. 7. H&E (A) and Masson's Trichrome (B) staining of subcutaneously implanted electrospun membranes for 14 days. The PCL/gelatin membrane does not allow cell infiltration (C). Increasing numbers of macrophages and multinucleated foreign body giant cells (FBGCs) surrounding its interface are observed over time. In contrast, the PCL/gelatin/MgO membrane supports cell infiltration from both the muscle and skin sides into the interior of membranes (A). Many infiltrating macrophages but no FBGC are surrounding the PCL/gelatin/MgO membrane. Statistically, the PCL/gelatin/MgO membrane shows significantly greater intense cell infiltration depth compared with the PCL/gelatin membrane (C). Green arrows indicate macrophage fused FGBCs. Two-way ANOVA with Tukey's post hoc test, * indicates $p < 0.05$ vs. PCL/gelatin. The fibrous capsule thickness of the PCL/gelatin membrane is approximately 100 μm and is unchanged for 14 days, while the PCL/gelatin/MgO membrane results in a fibrous capsule with decreasing thickness over time (D). Two-way ANOVA with Tukey's post hoc test, * indicates $p < 0.05$ vs. PCL/gelatin/MgO day 3.

waste. Previous approaches to improve the pro-angiogenic properties of electrospun membranes were mainly through incorporating pro-angiogenic growth factors [28,51] and compounds [52] into nanofibers. Controlled release of VEGF from core-shell nanofibers enhances the angiogenesis of electrospun membranes in vivo [28]. However, long-term maintenance of growth factor bioactivity of electrospun membranes remains a significant challenge, which might be an obstacle to the road to off-the-shelf products for clinical applications. Herein, we demonstrate early capillary formation within subcutaneously implanted PCL/gelatin/MgO membrane 7 days after implantation, which develops to matured capillary networks after 28 days (Fig. 8C), indicating that MgO nanoparticles enable good pro-angiogenic properties to electrospun membranes in vivo. This is highly attractive because rapid vascularization of electrospun membranes allows them to be better integrated with host tissues and to experience normal remodeling in vivo. Although there is no head-to-head comparison between growth factor-incorporated and MgO-incorporated electrospun membranes, we might conclude that they have equivalent pro-angiogenic properties by comparing blood vessel formation within implanted membranes. In comparison to pro-angiogenic growth factors, MgO is of low cost, long-term stability, and ease to be incorporated into nanofibers, making it more attractive for promoting

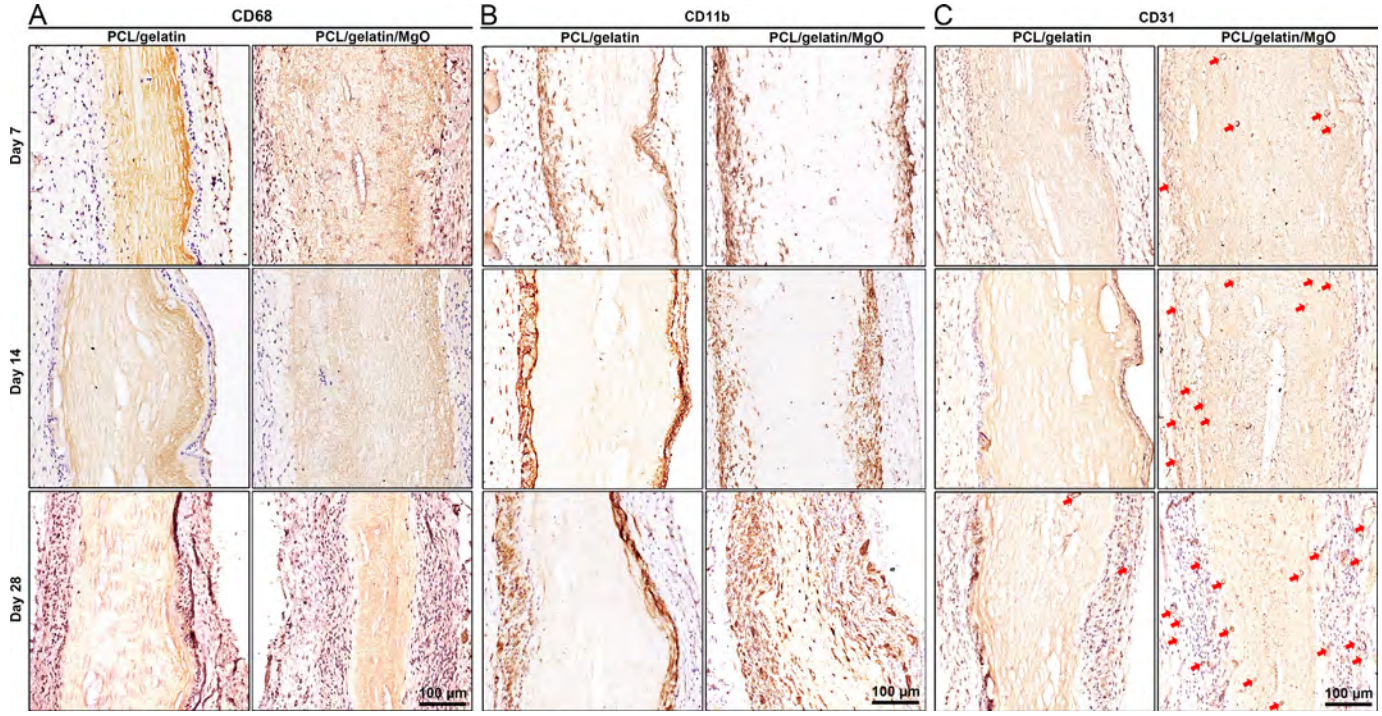

Fig. 8. Immunohistochemical staining for CD68+ (A), CD11b + (B), and CD31+ (C) of subcutaneously implanted electrospun membranes for 28 days. CD68+ pan-macrophages are localized at the exterior of fibrous capsule in the PCL/gelatin group and gradually decrease from day 7 to day 14 (A). While CD68+ pan-macrophages are generally distributed within the fibrous capsule surrounding the PCL/gelatin/MgO membrane at day 7 and disappear at day 14. After 28 days, both electrospun membranes are surrounded by dense layers of CD68+ pan-macrophages. Strikingly, the PCL/gelatin/MgO membrane shows a reduced thickness with the degraded counterparts being occupied by CD68+ pan-macrophages and fibroblasts at day 28. CD11b + leukocytes are mainly localized on the edge of the PCL/gelatin membrane at days 7 and 14 and partially infiltrate into its interior at day 28 (B). Infiltrated CD11b + cells into the PCL/gelatin/MgO membrane can be found at day 7 but they do not show further infiltration at day 14. Intense infiltration of CD11b + cells from the muscle and skin sides almost crosses the full thickness of the PCL/gelatin/MgO membrane at day 28. There is no evident capillary formation within the PCL/gelatin membrane after 28 days (C). In contrast, newly formed capillaries at the membrane-tissue interfaces and within the PCL/gelatin/MgO membrane are observed as early as day 7, thereafter, increased numbers of capillaries are observed from day 14 to day 28. Red arrows indicate newly formed capillaries.

angiogenesis of electrospun membranes. Despite this, the mechanism underlying great pro-angiogenic properties of MgO-incorporated membranes is not understood. Vascular endothelial cells are the predominant cellular population contributing to vascularization and angiogenesis and have been widely used to assess pro-angiogenic properties [28,53]. Mg^{2+} shows a concentration-dependent effect on promoting vascular endothelial cell proliferation [54]. The PCL/gelatin/MgO membrane significantly promoted HUVEC proliferation (Fig. 3D) and stimulated its production of VEGF (Fig. 3E). We therefore postulate that released Mg^{2+} from PCL/gelatin/MgO membrane recruits vascular endothelial cells and progenitor/stem cells and stimulates them to form vasculature in situ, as well as escalates other angiogenesis cascades.

Impairment in diabetic wound healing is attributed to aberrant inflammatory response, insufficient granulation tissue formation, and poor vascular regeneration [55]. Dysfunctional macrophages with imbalanced M1/M2 switch cause chronic inflammation that impairs the microenvironment of diabetic wounds [56]. Persistent abnormal inflammation is accompanied by excessive production of pro-inflammatory cytokines such as IL-1β, TNF-α, and IL-6, which were destructive to key effector cells, fibroblasts, endothelial cells, and keratinocytes, participating in the wound healing process [57]. Our data demonstrate that the PCL/gelatin/MgO membrane displays a systematic role in reverting dysfunctional macrophage phenotype switch. It stimulates macrophages differentiation toward M2 pro-healing phenotypes (Fig. 7B) and mitigates inflammatory responses as evidenced by downregulated gene expression of IL-1β and TNF-α (Fig. 4C) in the wounds of diabetic rats. M2-polarized macrophages produce more VEGF and TGF-β1, which reverses impaired angiogenesis and collagen accumulation [55]. In addition to mobilizing macrophages to promote angiogenesis and extracellular matrix production, the PCL/gelatin/MgO membrane directly target fibroblasts and endothelial cells to stimulate cell proliferation as well as to enhance growth factor and extracellular matrix accumulation for improved wound healing (Fig. 3). Therefore, the PCL/gelatin/MgO membrane provides good bioactivity that systematically improves the impaired diabetic wound microenvironments and accelerates wound healing of diabetic rats.

Biocompatibility is the primary prerequisite for designing biomaterial implants and medical devices. PCL is an ester polymer with good biocompatibility and has been approved by the U.S. Food and Drug Administration for fabricating many biomedical devices [58,59]. Gelatin is a mixture of peptides and proteins prepared through partial hydrolysis of collagen derived from various tissues/organs of animals. Previously, we and other groups have demonstrated that electrospun gelatin-based membranes are of good biocompatibility in many preclinical studies [60–63]. In line with those findings, we hereby confirm that the electrospun PCL/gelatin membrane did not elicit severe immune responses or complications. The formation of fibrous capsules is one of the characteristic hallmarks of FBR to biomaterial implants [43]. The PCL/gelatin membrane induced a fibrous capsule with a thickness of 100 μm (Fig. 7D), which is similar to that of many known biocompatible implants and devices [64–67]. We observed slightly elevated FBR for the implanted PCL/gelatin/MgO membrane in the first week as evidenced by a thicker fibrous capsule (Fig. 7D) and denser macrophage population (Fig. 8A and B). This is probably due to MgO hydrolysis that creates an alkaline environment and temporarily escalates local inflammatory responses. Alternatively, it might be associated with the burse release of magnesium ions (Fig. 2A) because higher concentrations of magnesium ions are toxic to cells and tissues [36,37]. Or, it can result from combinational detrimental effects of MgO hydrolysis products, magnesium hydroxide, and higher concentrations of magnesium ion, similar

to the toxic effects of commercial magnesium alloys [15,17,68]. Interestingly, the PCL/gelatin/MgO membrane showed gradually resolved inflammatory responses at days 7 and 14 compared with that of day 3, which is likely due to decreased amounts of MgO nanoparticles in the later stage of implantation. Our future study will replace MgO nanoparticles with magnesium salts at various concentrations to avoid alkaline products and over-accumulated magnesium ions. By a head-to-head comparison between MgO-incorporated membranes and magnesium salt-incorporated membranes, we might determine how does the slightly higher inflammatory response occur. In addition, evaluation of in vivo safety should be conducted by examining the major organs after implantation of the PCL/gelatin/MgO membrane [69].

A limitation of this study should be noted. A relatively small number of STZ-induced diabetic rats was used, which is not helpful to make a strong statistical evaluation. Such a small sample size is used because the PCL/gelatin/MgO membrane showed a striking promotive effect on diabetic wound healing compared with the control group in a pilot study. In addition, we performed another study involving the use of electrospun membranes containing magnesium salt to treat diabetic wounds and found similar exciting outcomes (unpublished data). For the sake of minimal use of animals, we only used three animals for each group at every endpoint.

5. Conclusions

The incorporation of MgO nanoparticles greatly increases the bioactivity of electrospun membranes and improves their physicochemical properties. MgO-incorporated membranes show promotive effects on the proliferation of vascular endothelial cells and upregulate their production of pro-angiogenic growth factors. The PCL/gelatin/MgO membrane alleviates inflammatory response, upregulates M1 to M2 switch of macrophages, and promotes granulation tissue formation, leading to accelerated wound healing of diabetic wounds. Incorporated MgO nanoparticles accelerate the degradation profile and augment the angiogenesis of electrospun membranes in vivo. These data indicate that MgO nanoparticles could be alternative to commonly used pro-angiogenic growth factors for enhancing angiogenesis of electrospun membranes that might serve as wound dressings for diabetic wounds.

Supplementary data to this article can be found online at https://doi.org/10.1016/j.msec.2021.112609.

CRediT authorship contribution statement

Jinglei Wu and Mingyue Liu designed the study and wrote the manuscript. Mingyue Liu, Ruilan Wang, Jiajie Liu, Weixing Zhang, Haiyan Li, Xiaoyu Wang, and Zhengni Liu performed the experiments. Jinglei Wu, Rui Zheng, Mingyue Liu, Ruilan Wang, Jiajie Liu, Weixing Zhang, Zhengni Liu, Xiangxin Lou, Huali Nie, Hongsheng Wang, Ahmed I. Abd-Elhamid, and Xiumei Mo analyzed and interpreted the data. All authors discussed the results and approved the final version of this manuscript.

Declaration of competing interest

The authors declare no competing financial interest.

Acknowledgements

The authors thank supports from Donghua University (2232019D3-20), National Natural Science Foundation of China (31900949), Science and Technology Commission of Shanghai Municipality (19440741300, 20ZR1401200, 18ZR1401800), and Cross Disciplinary Research Fund of Shanghai Ninth People's Hospital, Shanghai Jiao Tong University School of Medicine (JYJC202105).

References

[1] S. Balaji, S.S. Vaikunth, S.A. Lang, A.Q. Sheikh, F.Y. Lim, T.M. Crombleholme, D.A. Narmoneva, Tissue-engineered provisional matrix as a novel approach to enhance diabetic wound healing, Wound Repair Regen. 20 (2012) 15–27.
[2] V.T. Nguyen, N. Farman, R. Palacios-Ramirez, M. Sbeih, F. Behar-Cohen, S. Aractingi, F. Jaisser, Cutaneous wound healing in diabetic mice is improved by topical mineralocorticoid receptor blockade, J. Invest. Dermatol. 140 (2020) 223–234 e227.
[3] S. Avitabile, T. Odorisio, S. Madonna, S. Eyerich, L. Guerra, K. Eyerich, G. Zambruno, A. Cavani, F. Cianfarani, Interleukin-22 promotes wound wepair in wiabetes by improving keratinocyte pro-healing functions, J. Invest. Dermatol. 135 (2015) 2862–2870.
[4] H. Brem, A. Kodra, M.S. Golinko, H. Entero, O. Stojadinovic, V.M. Wang, C.M. Sheahan, A.D. Weinberg, S.L. Woo, H.P. Ehrlich, M. Tomic-Canic, Mechanism of sustained release of vascular endothelial growth factor in accelerating experimental diabetic healing, J. Invest. Dermatol. 129 (2009) 2275–2287.
[5] W. Yan, H. Liu, X. Deng, Y. Jin, N. Wang, J. Chu, Acellular dermal matrix scaffolds coated with connective tissue growth factor accelerate diabetic wound healing by increasing fibronectin through PKC signalling pathway, J. Tissue Eng. Regen. Med. 12 (2018) e1461–e1473.
[6] C. Mohanty, J. Pradhan, A human epidermal growth factor-curcumin bandage bioconjugate loaded with mesenchymal stem cell for in vivo diabetic wound healing, Mater. Sci. Eng. C Mater. Biol. Appl. 111 (2020), 110751.
[7] Y. Yang, T. Xia, W. Zhi, L. Wei, J. Weng, C. Zhang, X. Li, Promotion of skin regeneration in diabetic rats by electrospun core-sheath fibers loaded with basic fibroblast growth factor, Biomaterials 32 (2011) 4243–4254.
[8] Y. Yang, T. Xia, F. Chen, W. Wei, C. Liu, S. He, X. Li, Electrospun fibers with plasmid bFGF polyplex loadings promote skin wound healing in diabetic rats, Mol. Pharm. 9 (2012) 48–58.
[9] W. Srifa, N. Kosaric, A. Amorin, O. Jadi, Y. Park, S. Mantri, J. Camarena, G.C. Gurtner, M. Porteus, Cas9-AAV6-engineered human mesenchymal stromal cells improved cutaneous wound healing in diabetic mice, Nat. Commun. 11 (2020) 2470.
[10] N. Sun, B. Ning, K.M. Hansson, A.C. Bruce, S.A. Seaman, C. Zhang, M. Rikard, C.A. DeRosa, C.L. Fraser, M. Wagberg, R. Fritsche-Danielson, J. Wikstrom, K.R. Chien, A. Lundahl, M. Holtta, L.G. Carlsson, S.M. Peirce, S. Hu, Modified VEGF-A mRNA induces sustained multifaceted microvascular response and accelerates diabetic wound healing, Sci. Rep. 8 (2018) 17509.
[11] L. Hu, J. Wang, X. Zhou, Z. Xiong, J. Zhao, R. Yu, F. Huang, H. Zhang, L. Chen, Exosomes derived from human adipose mensenchymal stem cells accelerates cutaneous wound healing via optimizing the characteristics of fibroblasts, Sci. Rep. 6 (2016) 32993.
[12] F.I. Wolf, A. Cittadini, Chemistry and biochemistry of magnesium, Mol. Asp. Med. 24 (2003) 3–9.
[13] M. Nabiyouni, T. Bruckner, H. Zhou, U. Gbureck, S.B. Bhaduri, Magnesium-based bioceramics in orthopedic applications, Acta Biomater. 66 (2018) 23–43.
[14] Z. Yuan, P. Wei, Y. Huang, W. Zhang, F. Chen, X. Zhang, J. Mao, D. Chen, Q. Cai, X. Yang, Injectable PLGA microspheres with tunable magnesium ion release for promoting bone regeneration, Acta Biomater. 85 (2019) 294–309.
[15] D. Tie, H. Liu, R. Guan, P. Holt-Torres, Y. Liu, Y. Wang, N. Hort, In vivo assessment of biodegradable magnesium alloy ureteral stents in a pig model, Acta Biomater. 116 (2020) 415–425.
[16] D. Zhao, F. Witte, F. Lu, J. Wang, J. Li, L. Qin, Current status on clinical applications of magnesium-based orthopaedic implants: a review from clinical translational perspective, Biomaterials 112 (2017) 287–302.
[17] M. Shahin, K. Munir, C. Wen, Y. Li, Magnesium matrix nanocomposites for orthopedic applications: a review from mechanical, corrosion, and biological perspectives, Acta Biomater. 96 (2019) 1–19.
[18] X.Y. Wang, M.Y. Liu, H.Y. Li, A.L. Yin, C.L. Xia, X.X. Lou, H.S. Wang, X.M. Mo, J.L. Wu, MgO-incorporated porous nanofibrous scaffold promotes osteogenic differentiation of pre-osteoblasts, Mater. Lett. 299 (2021), 130098.
[19] Z. Lin, J. Wu, W. Qiao, Y. Zhao, K.H.M. Wong, P.K. Chu, L. Bian, S. Wu, Y. Zheng, K.M.C. Cheung, F. Leung, K.W.K. Yeung, Precisely controlled delivery of magnesium ions thru sponge-like monodisperse PLGA/nano-MgO-alginate core-shell microsphere device to enable in-situ bone regeneration, Biomaterials 174 (2018) 1–16.
[20] Z. Yuan, Z. Wan, P. Wei, X. Lu, J. Mao, Q. Cai, X. Zhang, X. Yang, Dual-controlled release of icariin/Mg(2+) from biodegradable microspheres and their synergistic upregulation effect on bone regeneration, Adv. Healthc. Mater. 9 (2020), e2000211.
[21] Y. Lai, Y. Li, H. Cao, J. Long, X. Wang, L. Li, C. Li, Q. Jia, B. Teng, T. Tang, J. Peng, D. Eglin, M. Alini, D.W. Grijpma, G. Richards, L. Qin, Osteogenic magnesium incorporated into PLGA/TCP porous scaffold by 3D printing for repairing challenging bone defect, Biomaterials 197 (2019) 207–219.
[22] U. Adhikari, N.P. Rijal, S. Khanal, D. Pai, J. Sankar, N. Bhattarai, Magnesium incorporated chitosan based scaffolds for tissue engineering applications, Bioact. Mater. 1 (2016) 132–139.
[23] Z. Wu, K. Zheng, J. Zhang, T. Tang, H. Guo, A.R. Boccaccini, J. Wei, Effects of magnesium silicate on the mechanical properties, biocompatibility, bioactivity, degradability, and osteogenesis of poly(butylene succinate)-based composite scaffolds for bone repair, J. Mater. Chem. B 4 (2016) 7974–7988.
[24] L. Xu, R. Willumeit-Romer, B.J.C. Luthringer-Feyerabend, Effect of magnesium-degradation products and hypoxia on the angiogenesis of human umbilical vein endothelial cells, Acta Biomater. 98 (2019) 269–283.
[25] W. Lin, M. Chen, T. Qu, J. Li, Y. Man, Three-dimensional electrospun nanofibrous scaffolds for bone tissue engineering, J. Biomed. Mater. Res. B Appl. Biomater. 108 (2020) 1311–1321.
[26] T. Wu, X. Mo, Y. Xia, Moving electrospun nanofibers and bioprinted scaffolds toward translational applications, Adv. Healthc. Mater. 9 (2020), e1901761.
[27] P. Mikes, A. Broz, A. Sinica, N. Asatiani, L. Bacakova, In vitro and in vivo testing of nanofibrous membranes doped with alaptide and L-arginine for wound treatment, Biomed. Mater. 15 (2020), 065023.
[28] H. Zigdon-Giladi, A. Khutaba, R. Elimelech, E.E. Machtei, S. Srouji, VEGF release from a polymeric nanofiber scaffold for improved angiogenesis, J. Biomed. Mater. Res. A 105 (2017) 2712–2721.

[29] K. Huang, E.W. Ozpinar, T. Su, J. Tang, D. Shen, L. Qiao, S. Hu, Z. Li, H. Liang, K. Mathews, V. Scharf, D.O. Freytes, K. Cheng, An off-the-shelf artificial cardiac patch improves cardiac repair after myocardial infarction in rats and pigs, Sci. Transl. Med. 12 (2020) eaat9683.
[30] R. Augustine, E.A. Dominic, I. Reju, B. Kaimal, N. Kalarikkal, S. Thomas, Investigation of angiogenesis and its mechanism using zinc oxide nanoparticle-loaded electrospun tissue engineering scaffolds, RSC Adv. 4 (2014) 51528–51536.
[31] S.M. Eppler, D.L. Combs, T.D. Henry, J.J. Lopez, S.G. Ellis, J.H. Yi, B.H. Annex, E.R. McCluskey, T.F. Zioncheck, A target-mediated model to describe the pharmacokinetics and hemodynamic effects of recombinant human vascular endothelial growth factor in humans, Clin. Pharmacol. Ther. 72 (2002) 20–32.
[32] T.P. Richardson, M.C. Peters, A.B. Ennett, D.J. Mooney, Polymeric system for dual growth factor delivery, Nat. Biotechnol. 19 (2001) 1029–1034.
[33] N.P. Rijal, U. Adhikari, S. Khanal, D. Pai, J. Sankar, N. Bhattarai, Magnesium oxide-poly (ε-caprolactone)-chitosan-based composite nanofiber for tissue engineering applications, Mater. Sci. Eng. B 228 (2018) 18–27.
[34] A. Abdal-Ha, S. Hamlet, S. Ivanovski, Fabrication of a thick three-dimensional scaffold with an open cellular-like structure using airbrushing and thermal cross-linking of molded short nanofibers, Biofabrication 11 (2018), 015006.
[35] U. Adhikari, X. An, N. Rijal, T. Hopkins, S. Khanal, T. Chavez, R. Tatu, J. Sankar, K.J. Little, D.B. Hom, N. Bhattarai, S.K. Pixley, Embedding magnesium metallic particles in polycaprolactone nanofiber mesh improves applicability for biomedical applications, Acta Biomater. 98 (2019) 215–234.
[36] S. Ababzadeh, A. Farzin, A. Goodarzi, R. Karimi, M. Sagharjoghi Farahani, M. Eslami Farsani, K. Gharibzad, M. Zahiri, J. Ai, High porous electrospun poly(epsilon-caprolactone)/gelatin/MgO scaffolds preseeded with endometrial stem cells promote tissue regeneration in full-thickness skin wounds: an in vivo study, J. Biomed. Mater. Res. B Appl. Biomater. 108 (2020) 2961–2970.
[37] X. Liu, X. He, D. Jin, S. Wu, H. Wang, M. Yin, A. Aldalbahi, M. El-Newehy, X. Mo, J. Wu, A biodegradable multifunctional nanofibrous membrane for periodontal tissue regeneration, Acta Biomater. 108 (2020) 207–222.
[38] M. Liu, X. Wang, H. Li, C. Xia, Z. Liu, J. Liu, A. Yin, X. Lou, H. Wang, X. Mo, J. Wu, Magnesium oxide-incorporated electrospun membranes inhibit bacterial infections and promote the healing process of infected wounds, J. Mater. Chem. B 9 (2021) 3727–3744.
[39] B. Feng, H. Tu, H. Yuan, H. Peng, Y. Zhang, Acetic-acid-mediated miscibility toward electrospinning homogeneous composite nanofibers of GT/PCL, Biomacromolecules 13 (2012) 3917–3925.
[40] R. Xu, H. Xia, W. He, Z. Li, J. Zhao, B. Liu, Y. Wang, Q. Lei, Y. Kong, Y. Bai, Z. Yao, R. Yan, H. Li, R. Zhan, S. Yang, G. Luo, J. Wu, Controlled water vapor transmission rate promotes wound-healing via wound re-epithelialization and contraction enhancement, Sci. Rep. 6 (2016) 24596.
[41] B.L. Furman, Streptozotocin-induced diabetic models in mice and rats, Curr. Protoc. Pharmacol. 70 (2015) (5 47 41-45 47 20).
[42] N.J. Darling, W. Xi, E. Sideris, A.R. Anderson, C. Pong, S.T. Carmichael, T. Segura, Click by click microporous annealed particle (MAP) scaffolds, Adv. Healthc. Mater. 9 (2020), e1901391.
[43] P.T. Thevenot, A.M. Nair, J. Shen, P. Lotfi, C.Y. Ko, L. Tang, The effect of incorporation of SDF-1alpha into PLGA scaffolds on stem cell recruitment and the inflammatory response, Biomaterials 31 (2010) 3997–4008.
[44] H. Cai, J. Meng, X. Li, F. Xue, C. Chu, C. Guo, J. Bai, In vitro degradation behavior of Mg wire/poly(lactic acid) composite rods prepared by hot pressing and hot drawing, Acta Biomater. 98 (2019) 125–141.
[45] E. Girard, G. Chagnon, A. Moreau-Gaudry, C. Letoublon, D. Favier, S. Dejean, B. Trilling, B. Nottelet, Evaluation of a biodegradable PLA-PEG-PLA internal biliary stent for liver transplantation: in vitro degradation and mechanical properties, J. Biomed. Mater. Res. B Appl. Biomater. 109 (2021) 410–419.
[46] Y. Zare, K.Y. Rhee, S.J. Park, Simple model for hydrolytic degradation of poly(lactic acid)/poly(ethylene oxide)/carbon nanotubes nanobiosensor in neutral phosphate-buffered saline solution, J. Biomed. Mater. Res. A 107 (2019) 2706–2717.
[47] A. Ferrandez-Montero, M. Lieblich, J.L. Gonzalez-Carrasco, R. Benavente, V. Lorenzo, R. Detsch, A.R. Boccaccini, B. Ferrari, Development of biocompatible and fully bioabsorbable PLA/Mg films for tissue regeneration applications, Acta Biomater. 98 (2019) 114–124.
[48] C. Del Gaudio, S. Baiguera, M. Boieri, B. Mazzanti, D. Ribatti, A. Bianco, P. Macchiarini, Induction of angiogenesis using VEGF releasing genipin-crosslinked electrospun gelatin mats, Biomaterials 34 (2013) 7754–7765.
[49] X. Chen, D. Chen, X. Ai, R. Hu, H. Zhang, A new method for the preparation of three-layer vascular stents: a preliminary study on the preparation of biomimetic three-layer vascular stents using a three-stage electrospun membrane, Biomed. Mater. 15 (2020), 055010.
[50] M.W. Laschke, Y. Harder, M. Amon, I. Martin, J. Farhadi, A. Ring, N. Torio-Padron, R. Schramm, M. Rucker, D. Junker, J.M. Haufel, C. Carvalho, M. Heberer, G. Germann, B. Vollmar, M.D. Menger, Angiogenesis in tissue engineering: breathing life into constructed tissue substitutes, Tissue Eng. 12 (2006) 2093–2104.
[51] C. Zhang, J. Wang, Y. Xie, L. Wang, L. Yang, J. Yu, A. Miyamoto, F. Sun, Development of FGF-2-loaded electrospun waterborne polyurethane fibrous membranes for bone regeneration, Regen. Biomater. 8 (2021), rbaa046.
[52] S. Asadpour, H. Yeganeh, F. Khademi, H. Ghanbari, J. Ai, Resveratrol-loaded polyurethane nanofibrous scaffold: viability of endothelial and smooth muscle cells, Biomed. Mater. 15 (2019), 015001.
[53] Y. Yuan, S. Khan, D.J. Stewart, D.W. Courtman, Engineering blood outgrowth endothelial cells to optimize endothelial nitric oxide synthase and extracellular matrix production for coating of blood contacting surfaces, Acta Biomater. 109 (2020) 109–120.
[54] N. Zhao, D. Zhu, Endothelial responses of magnesium and other alloying elements in magnesium-based stent materials, Metallomics 7 (2015) 118–128.
[55] Y. Ishida, Y. Kuninaka, M. Nosaka, M. Furuta, A. Kimura, A. Taruya, H. Yamamoto, E. Shimada, M. Akiyama, N. Mukaida, T. Kondo, CCL2-mediated reversal of impaired skin wound healing in diabetic mice by normalization of neovascularization and collagen accumulation, J. Invest. Dermatol. 139 (2019) 2517–2527 e2515.
[56] J. Hu, L. Zhang, C. Liechty, C. Zgheib, M.M. Hodges, K.W. Liechty, J. Xu, Long noncoding RNA GAS5 regulates macrophage polarization and diabetic wound healing, J. Invest. Dermatol. 140 (2020) 1629–1638.
[57] T. Shen, K. Dai, Y. Yu, J. Wang, C. Liu, Sulfated chitosan rescues dysfunctional macrophages and accelerates wound healing in diabetic mice, Acta Biomater. 117 (2020) 192–203.
[58] J.C. Silva, R.N. Udangawa, J. Chen, C.D. Mancinelli, F.F.F. Garrudo, P.E. Mikael, J.M.S. Cabral, F.C. Ferreira, R.J. Linhardt, Kartogenin-loaded coaxial PGS/PCL aligned nanofibers for cartilage tissue engineering, Mater. Sci. Eng. C Mater. Biol. Appl. 107 (2020), 110291.
[59] K. Paul, S. Darzi, G. McPhee, M.P. Del Borgo, J.A. Werkmeister, C.E. Gargett, S. Mukherjee, 3D bioprinted endometrial stem cells on melt electrospun poly epsilon-caprolactone mesh for pelvic floor application promote anti-inflammatory responses in mice, Acta Biomater. 97 (2019) 162–176.
[60] B. Feng, S. Wang, D. Hu, W. Fu, J. Wu, H. Hong, I.J. Domian, F. Li, J. Liu, Bioresorbable electrospun gelatin/polycaprolactone nanofibrous membrane as a barrier to prevent cardiac postoperative adhesion, Acta Biomater. 83 (2019) 211–220.
[61] O. Gil-Castell, J.D. Badia, I. Ontoria-Oviedo, D. Castellano, P. Sepulveda, A. Ribes-Greus, Polycaprolactone/gelatin-based scaffolds with tailored performance: in vitro and in vivo validation, Mater. Sci. Eng. C Mater. Biol. Appl. 107 (2020), 110296.
[62] X. Xie, D. Li, Y. Chen, Y. Shen, F. Yu, W. Wang, Z. Yuan, Y. Morsi, J. Wu, X. Mo, Conjugate electrospun 3D gelatin nanofiber sponge for rapid hemostasis, Adv. Healthc. Mater. 10 (2021), e2100918.
[63] H. Li, X. Wang, J. Liu, Z. Liu, H. Wang, X. Mo, J. Wu, Nanofiber configuration affects biological performance of decellularized meniscus extracellular matrix incorporated electrospun scaffolds, Biomed. Mater. 16 (2021), 065013.
[64] R.H. Raeder, S.F. Badylak, C. Sheehan, B. Kallakury, D.W. Metzger, Natural anti-galactose α1,3 galactose antibodies delay, but do not prevent the acceptance of extracellular matrix xenografts, Transplant. Immunol. 10 (2002) 15–24.
[65] J.E. Valentin, N.J. Turner, T.W. Gilbert, S.F. Badylak, Functional skeletal muscle formation with a biologic scaffold, Biomaterials 31 (2010) 7475–7484.
[66] S. Mirsadraee, H.E. Wilcox, K.G. Watterson, J.N. Kearney, J. Hunt, J. Fisher, E. Ingham, Biocompatibility of acellular human pericardium, J. Surg. Res. 143 (2007) 407–414.
[67] D.M. Higgins, R.J. Basaraba, A.C. Hohnbaum, E.J. Lee, D.W. Grainger, M. Gonzalez-Juarrero, Localized immunosuppressive environment in the foreign body response to implanted biomaterials, Am. J. Pathol. 175 (2009) 161–170.
[68] P. Xiong, J. Yan, P. Wang, Z. Jia, W. Zhou, W. Yuan, Y. Li, Y. Liu, Y. Cheng, D. Chen, Y. Zheng, A pH-sensitive self-healing coating for biodegradable magnesium implants, Acta Biomater. 98 (2019) 160–173.
[69] F. Zhang, X. Han, C. Guo, H. Yang, J. Wang, X. Wu, Fibrous aramid hydrogel supported antibacterial agents for accelerating bacterial-infected wound healing, Mater. Sci. Eng. C Mater. Biol. Appl. 121 (2021), 111833.